

Deformation behaviour of electrodeposited nanocrystalline Ni with broad grain size distribution

W. C. Xu¹, P. Q. Dai*¹ and X. L. Wu²

In the present work, nanocrystalline Ni (nc-Ni) with a broad grain size distribution (BGSD) of 5–120 nm and an average grain size of 27.2 nm was prepared. The BGSD nc-Ni sample shows a similar strength and good ductility in comparison with electrodeposited nc-Ni with a narrow grain size distribution. The intracrystalline dislocation network was observed in the post-deformed microstructure confirming the conventional intracrystalline dislocation sliding mechanism in BGSD nc-Ni. The uniaxial tensile loading–unloading–loading deformation shows BGSD nc-Ni has the capability to store dislocations in the grain interior, which is very limited compared with that of coarse grained metals. For BGSD nc-Ni, the strain rate sensitivity of flow stress m enhances with decreasing strain rate. At the strain rate of $5 \times 10^{-6} \text{ s}^{-1}$, m was estimated to be 0.055. At the corresponding strain rate, the enhanced ductility along with the decreased strength was achievable, indicating activation of other deformation mechanisms, e.g. grain boundary sliding or diffusion.

Keywords: Nanocrystalline Ni, Grain size distribution, Dislocation, Strain rate sensitivity, Grain growth, Jump test

Introduction

Nanocrystalline (nc) materials with high strength and high hardness, are expected to be new generation engineering structural materials, but obtaining higher ductility must be the premise of practice applications. In the past decade, deformation mechanisms in nc materials were extensively investigated through experimental studies and molecular dynamics simulations. Some new deformation mechanisms, including partial dislocations emission from grain boundaries (GBs),¹ deformation twin,^{1,2} grain rotation,³ GB migration,⁴ have been well proposed. However, the direct relationship between deformation mechanisms and associated mechanical properties, especially for the ductility, is not fully understood yet. Nonetheless, some effective routes have been suggested to improve the ductility of nc materials.^{5–8} One of these routes was focused on the microstructure design, e.g. a composition of nanoscale grains and ultrafine grains (UFGs) (100–500 nm).^{5,7} This means relying on the nc matrix to hold the high strength, but this increases ductility by introduction of the conventional dislocation sliding into large grains. According to the characteristic of nc materials having abnormal grain growth, the bimodal microstructure can be obtained by thermal annealing. For electrodeposited nc metals,

however, low temperature annealing always causes embrittlement.⁹ Recently, Shen and coworkers¹⁰ prepared a special electrodeposited nc-Ni with a broad grain size distribution (BGSD). The nc-Ni sample had the upper limit of grain size over 160 nm but with an average grain size of 37 nm in the as deposited statement. The combination of high strength and good ductility was reported for the BGSD nc-Ni sample. Because the BGSD nc-Ni sample was prepared by an unopened process, many associated studies fail to be extensively investigated. In the present study, the BGSD nc-Ni samples were successfully prepared by the present process and also showed high strength along with good ductility. The intracrystalline dislocation network was observed in the post-deformed microstructures confirming the conventional intracrystalline dislocation sliding mechanism. The effects of strain rates on mechanical properties and strain rate sensitivity of flow stress m were studied. In addition, the uniaxial tensile loading–unloading–loading process was also conducted.

Experimental procedure

In the present study, an aqueous sulphamate-based electrolyte was used to produce BGSD nc-Ni by direct current electrodeposition. The electrolyte was made of $500 \text{ g L}^{-1} \text{ Ni}(\text{NH}_2\text{SO}_3)_2 \cdot 4\text{H}_2\text{O}$, $20 \text{ g L}^{-1} \text{ NiCl}_2 \cdot 6\text{H}_2\text{O}$, 30 g L^{-1} boric acid, 2.5 g L^{-1} soluble saccharin, 0.1 g L^{-1} sodium lauryl sulphate and a small amount of special additives. The main electrodeposition conditions are listed in Table 1. Under these conditions, BGSD nc-Ni, the thickness of which was 180–200 μm ,

¹College of Materials Science and Engineering, Fuzhou University, Fuzhou 350108, China

²State Key Laboratory of Nonlinear Mechanics, Institute of Mechanics, Chinese Academy of Sciences, Beijing 100080, China

*Corresponding author, email pqdai@126.com

was deposited on stainless steel substrates, which had been polished to a mirror-like finish surface before electrodeposition. After electrodeposition, the deposits can be mechanically stripped from stainless steels.

The microstructures of BGSD nc-Ni were observed by transmission electronic microscope (TEM). Transmission electronic microscopy observations were performed using a Tecnai G2 F20 S-TWIN operated at 200 kV. Transmission electronic microscopy samples were prepared by double jet electropolishing using an electrolyte consisting of 5 vol.-% perchloric acid and 95 vol.-% ethanol at a temperature below -20°C . The TEM average grain size was determined from dark field TEM images using the image analysis software (Photoshop 7.0) to count at least 500 grains for each sample.

The dog bone shaped tensile specimens of BGSD nc-Ni, with a gauge length of 10 mm and gauge width of 3 mm, were cut using an electrodischarging machine. The room temperature (RT) tensile tests were carried out with the strain rate varying from 10^{-5} to 10^{-3} s^{-1} . For determination of m , a strain rate change (jump) test was carried out. For comparison, a coarse grained Ni (CG-Ni) sample with an average grain size of 60 μm , which was measured by the line intercept method, was used. The CG-Ni tensile sample with a thickness of 1 mm had an identical as machined geometry as that of BGSD nc-Ni.

Results and discussion

The TEM bright field image of the as deposited nc-Ni sample is shown in Fig. 1a. It is observed that isolated large grains (up to 120 nm) are surrounded by small grains (<30 nm) forming an inhomogeneous microstructure, which is similar to grains undergone abnormal growth in the low temperature annealing. Some defects (dislocation, twin or subgrain boundary), marked by black arrows in Fig. 1a, are clearly seen within the large grains. The inset in Fig. 1a is a typical ring pattern further confirming that the global grain size is in the nanoscale. The average grain size and the grain size distribution were obtained by counting grains from TEM dark field images, which were similar to Fig. 1b. The statistical diagram in Fig. 1c shows that the BGSD nc-Ni sample has an average grain size of 27.2 nm with a grain size distribution ranging from 5 to 120 nm.

The engineering stress–strain σ – ϵ curves with strain rates of 10^{-5} to 10^{-3} s^{-1} for BGSD nc-Ni are shown in Fig. 2. It shows a strong strain rate dependence of strength and ductility. The 0.2% offset yield strength $\sigma_{0.2}$ (marked by open circle in the curves) and the ultimate tensile strength σ_{UTS} both increase significantly with increasing strain rate. $\sigma_{0.2}$ is increased from 523 to 698 MPa, and σ_{UTS} is increased from 1032 to 1246 MPa. The elongation to fracture δ_{ETF} enhances significantly with decreasing strain rate. The δ_{ETF} is

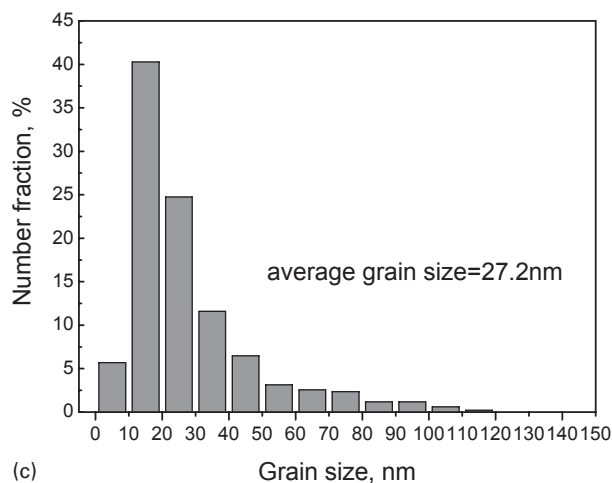
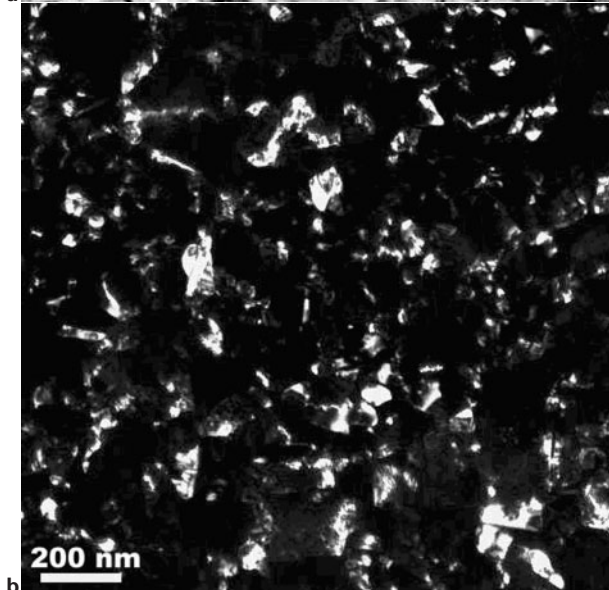
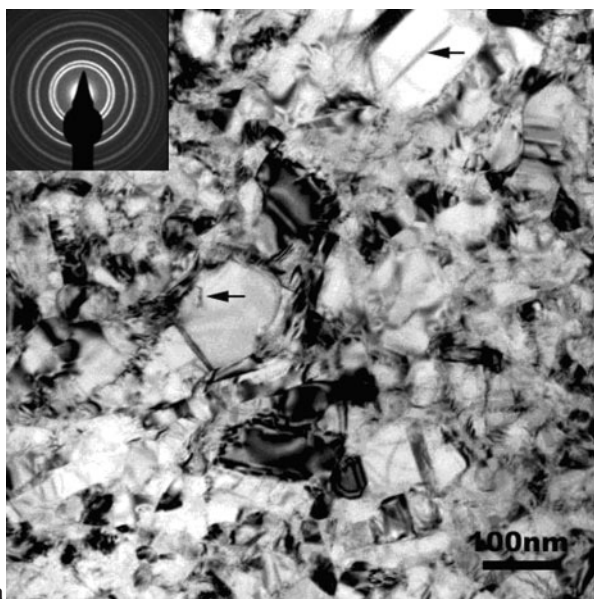
enhanced from 9.45 to 13.35%. In comparison with nc-Ni, with a relatively narrow grain size distribution (NGSD) of 10–50 nm and an average grain size of 15–25 nm, which has a high strength with σ_{UTS} of 1200–1300 MPa and a common ductility with δ_{ETF} of $\sim 4\%$ at RT and strain rates of 3×10^{-3} or 10^{-4} s^{-1} ,¹¹ apparently, the present BGSD nc-Ni samples possess the markedly enhanced ductility and the similar strength at RT and approaching strain rates. The BGSD nc-Ni samples with a grain size distribution of 10–160 nm and an average grain size of 37 nm prepared by Shen *et al.*, have a very high σ_{UTS} of 1400–1916 MPa and δ_{ETF} of 5.6–11.3% at strain rates of 1.35×10^{-6} to 1.35 s^{-1} .¹⁰ Our BGSD nc-Ni and common NGSD nc-Ni follow the Hall–Petch relationship very well, while the nc-Ni of Shen *et al.* shows a surprisingly inverse Hall–Petch relationship. Nevertheless, the BGSD nc-Ni samples from the authors and Shen *et al.* both display a strong strain rate dependence of strength and ductility.

Figure 3a shows a TEM bright field image from the tensile fracture of BGSD nc-Ni at the strain rate of 10^{-4} s^{-1} . Apparent grain growth is observed in contrary to the as deposited grain size in Fig. 1a. In comparison with Fig. 1c, the statistical analysis in Fig. 3b displays that the average grain size after deformation is increased by 19.3 nm and that there is a sharp decrease in the number fraction of sizes below 30 nm. In addition, few large grain coalescences with sizes over 200 nm are also observed in the post-deformed microstructures, as shown in Fig. 3c. These observations indicate that the propensity of grain growth driven by applied stresses in BGSD nc-Ni is stronger than that of NGBD nc-Ni.^{3,4,12} It seems that the large grains can act as cores to merge neighbouring small grains by grain rotation^{3,12} forming the grain coalescence during plastic deformation. In addition, dislocations trapped in the grain coalescence and dislocation pile-ups at GBs are also observed. One of these phenomena was captured in Fig. 3c. These findings offer compelling evidence to support the conventional intracrystalline dislocation sliding mechanism dominated in BGSD nc-Ni.

It was pointed that dislocations are hardly to move in small nanograins due to the need of very high stress to activate dislocation sources, e.g. the Frank–Read source.¹³ The critical stress τ to activate the Frank–Read source can be expressed as $\tau = Gb/L$, where G is shear module (80 GPa for Ni), b the smallest Burgers vector in face centred cubic metals (0.249 nm for Ni) and L the distance between two pinning points (typical $L = d/3$ or $d/4$ and d is the grain diameter). According to the equation, for grains with sizes of 80–120 nm, τ is estimated to be about 498–746 MPa, which is close to the present experimental yield stress. Accordingly, the Frank–Read source can be activated in the large grains of sizes over 80 nm in the practical tensile deformation. Moreover, grain growth in the plastic deformation

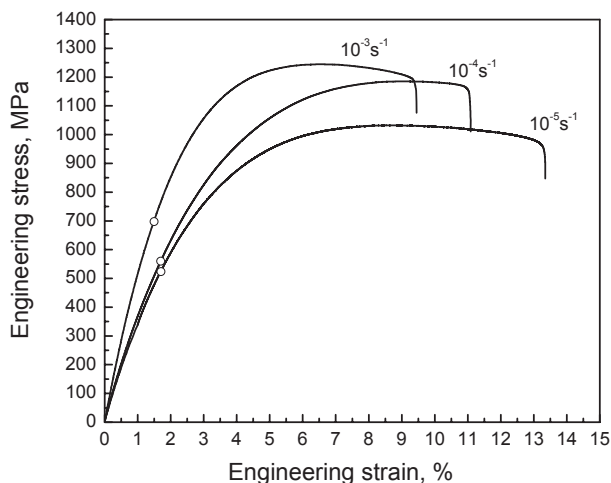
Table 1 Main electrodeposition conditions for preparing BGSD nc-Ni

Electrolyte volume, L	1
Electrolyte temperature, $^{\circ}\text{C}$	60
pH	3.5
Current density, A dm^{-2}	8
Anode material	Electrolytic Ni (purity >99.9 mass-%)
Ratio of cathode area to anode area in the plating bath	1:4
Cathode substrate	Stainless steel sheet (1Cr15Mn8Ni5Cu2)



a bright field image and corresponding selected area electron diffraction pattern; b dark field image; c statistical diagram of grain size

1 Images (TEM) of microstructures and statistical grain size distribution of BGSD nc-Ni



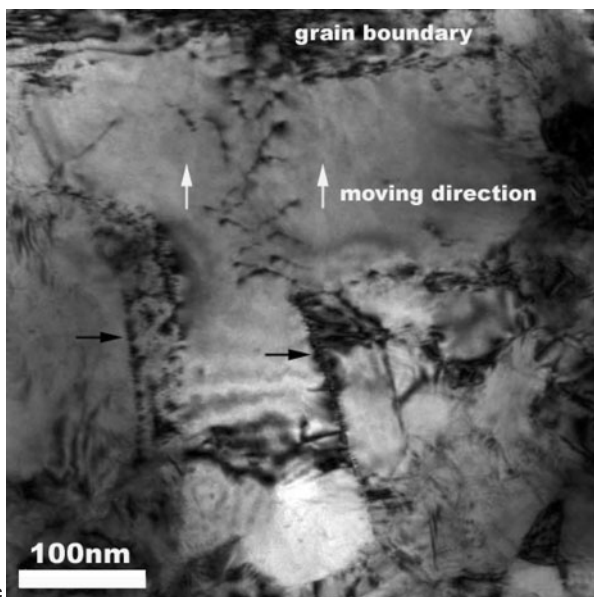
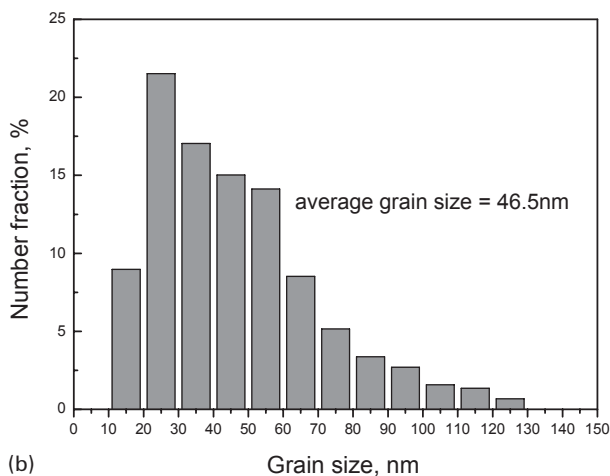
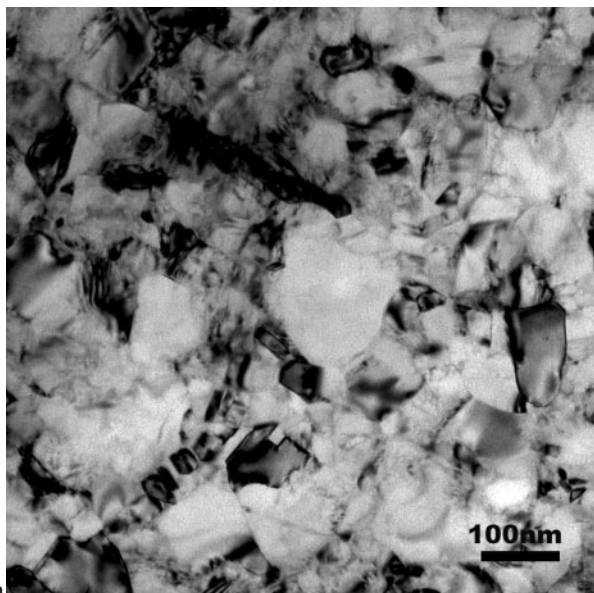
2 Engineering stress-strain curves with strain rates from 10^{-5} to 10^{-3} s^{-1} for BGSD nc-Ni

process may further favour the activation of the Frank-Read source with increasing deformation strains.

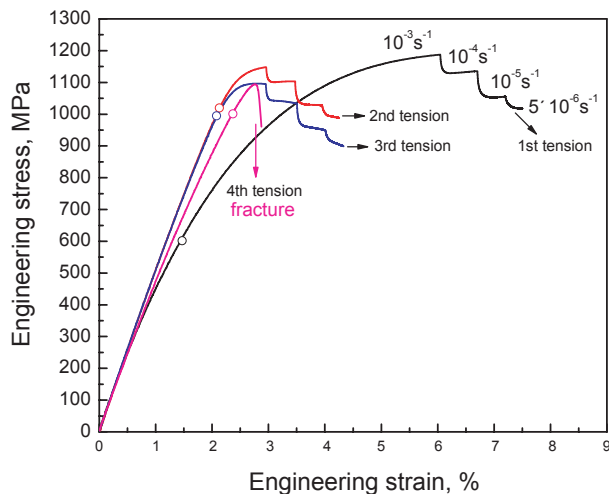
The repeated loading-unloading-reloading tensile curves accompanied with determination of m by down jump tests for BGSD nc-Ni are shown in Fig. 4. The starting jump point was selected at strain=6% in the first tensile deformation, assuring that the jump test was conducted at the plain stage of tensile curve. At each subsequent cyclic tensile deformation, the starting jump point was selected at strain=3% assuring that as many as the cyclic tensile deformation were carried out. In Fig. 4, an apparent increase in $\sigma_{0.2}$ ($\sim 400 \text{ MPa}$) is seen in the second tensile deformation, and $\sigma_{0.2}$ is kept constant ($\sim 1000 \text{ MPa}$) at the subsequent cyclic deformations, indicating the formation of a dislocation network with a saturated density during repeated loading-unloading-reloading process. Although BGSD nc-Ni has the capability to store dislocations in the grain interior according to the variation of $\sigma_{0.2}$ present in the cyclic tensile deformation, it is very limited compared with that of CG metals. However, for NGSD nc-Ni, it has no capability to store dislocations because no dislocation debris was detected in repeated loading-unloading-reloading tensile deformation.¹⁴

The plots of m versus strain rate for BGSD nc-Ni and CG-Ni are shown in Fig. 5a. Figure 5b and c shows the stress-strain curve under the up jump test for BGSD nc-Ni and CG Ni. The up jump tests were performed in the strain rates from 10^{-5} to 10^{-3} s^{-1} with an increased rate of 2- or 2.5-fold. The starting point of up jump test was selected at strain=5% for BGSD nc-Ni, where the tensile deformation has entered into the plain stage. An obvious variation of flow stresses can be seen from the magnifying inset in Fig. 5b and c as the strain rate abruptly changes.

For the present CG-Ni, which has an average grain size of $\sim 60 \mu\text{m}$, m is kept constant (~ 0.008) in the experimental strain rate range. The result is in the same order as the reported m in another CG-Ni.¹⁵ For CG metals, m is insensitive to the strain rate and stable in the wide strain rate range responsible for the deformation controlled by slide dislocations cutting through dislocation forests.¹⁶ However, for BGSD nc-Ni, m shows a strong dependence of strain rate. As shown in Fig. 5a, m increases linearly from 0.018 to 0.037 with decreasing



a typical image showing pronounced grain growth; b statistical grain size distribution after deformation; c image showing significant grain coalescences and pile-ups of dislocation ahead of GBs after deformation
3 Images (TEM) of tensile fracture of BGSD nc-Ni sample at strain rate of 10^{-4} s^{-1} and statistical analysis of grain size



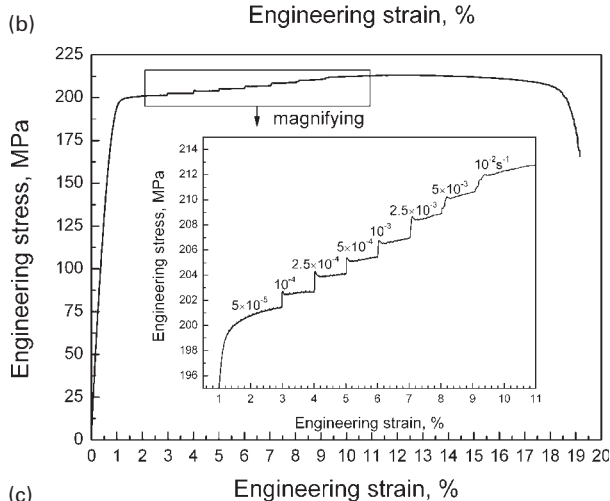
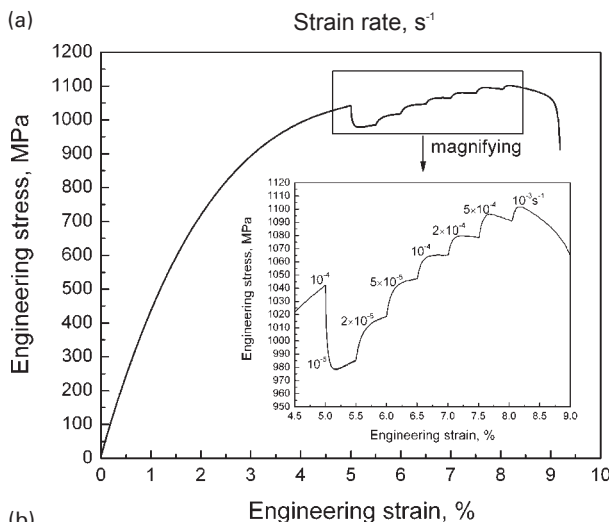
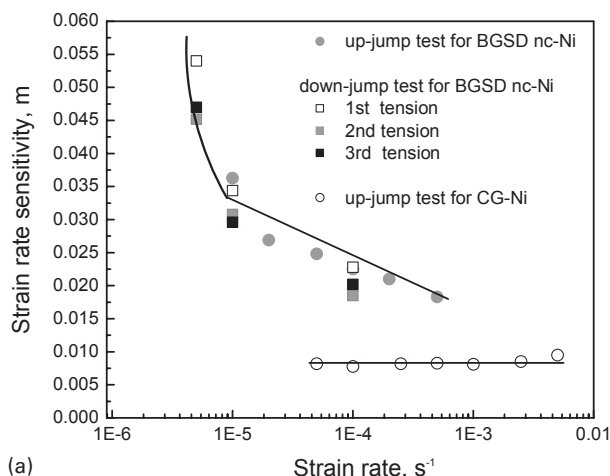
4 Repeated loading-unloading-reloading tensile curves accompanied with determination of strain rate sensitivity of flow stress m by down jump tests for BGSD nc-Ni: $\sigma_{0.2}$ was marked by open circle; unloading curves were not given here

strain rate from 10^{-5} to 10^{-3} s^{-1} . However, it seems that m increases exponentially with decreasing strain rate, as the strain rate is $< 10^{-3} \text{ s}^{-1}$. At the strain rate of $5 \times 10^{-6} \text{ s}^{-1}$, m is estimated to be 0.055, which is about 2–3 times of the value measured at the strain rate of 10^{-3} s^{-1} . For most NGSD nc-Ni, m is usually estimated to be 0.01–0.02 at the similar strain rates,^{15,17} and this m corresponds to a deformation process associated with dislocation emission from GBs^{1,9,11} but not conventional intracrystalline dislocation sliding. Although m of 0.018 obtained at the strain rate of 10^{-3} s^{-1} for BGSD nc-Ni is consistent with m of NGSD nc-Ni at the similar strain rate region, intracrystalline dislocation sliding, which was observed in the post-deformed microstructures shown in Fig. 3c, should play an important role in combination with partial dislocation emission from GBs for BGSD nc-Ni. The successively enhanced m with decreasing strain rate, especially for $m=0.055$ at the strain rate of $5 \times 10^{-6} \text{ s}^{-1}$, in BGSD nc-Ni indicates that other deformation mechanisms, e.g. diffusion and GB sliding, may be activated at very slow strain rates and even probably becomes a dominant mechanism together with the dislocation mechanism in the plastic deformation. High m value, e.g. 0.2–0.5, usually corresponds to a GB sliding related elevated temperature deformation mechanism like superplasticity.¹⁸

The occurrence of plastic instability can be judged by the famous Hart's criterion¹⁹

$$1/\sigma \cdot (\partial\sigma/\partial\epsilon)_\epsilon - 1 + m \leq 0$$

where $1/\sigma \cdot (\partial\sigma/\partial\epsilon)_\epsilon$ is also defined as a normalised strain hardening rate Θ .¹⁵ Thus, the Hart's criterion is also depicted as $\Theta - 1 + m \leq 0$. Apparently, Θ and m are two key factors that together affect plastic instability. Moreover, increasing Θ or m has been acted as an effective way to enhance ductility.²⁰ The effect of strain rate on the ductility of CG, UFG or nc metals shows many inconsistent results.^{10,21–23} It is believed that this is responsible for the competing result between Θ and m at different strain rates. For example, for a UFG Cu sample,²¹ m is nearly invariable at the strain rate region



5 a plots of m as function of strain rate for BGSD nc-Ni and CG-Ni (m was determined from Fig. 4 as well as Fig. 5b and c); engineering stress–strain curve obtained in strain rate change (jump) test for b BGSD nc-Ni and c CG-Ni: m was estimated as $m = (\partial \ln \sigma / \partial \ln \dot{\epsilon})_{\sigma}$, where $\dot{\epsilon}$ is the strain rate

of 1.04×10^{-5} – 1.04 s^{-1} , while Θ is enhanced with increasing strain rate resulting in a delay of plastic instability. Therefore, this UFG Cu sample shows the successively enhanced ductility with increasing strain rate. For CG metals, the ductility is often independent of the strain rate responsible for both m and Θ insensitive to strain rate.^{21,23} For the present BGSD nc-Ni sample, Θ should have a small change with the strain rate due to very limited strain hardening as the

perfectly plastic behaviour seen in Fig. 2. Therefore, enhanced m with increasing strain rate can favour delayed plasticity instability, leading to an expected enhancement of ductility, which is consistent with the result in Fig. 2. The enhanced m in a brush plated nc-Cu sample²² was primarily attributed to predominant high angle GBs. Ultrafine grain Cu with nanoscale twins, whose GB structure is equivalent to high angle GB, also shows a higher m .²⁴ In the present BGSD nc-Ni, high angle GBs are also predominant due to the well defined GB contrast in Fig. 1a. Consequently, high angle GBs for nc metals should be the main reason for high m . It is noted that, for BGSD nc-Ni subjected to the cyclic tensile deformation, m at the same strain rate decreases at the second tensile deformation and keeps nearly unchangeable at the subsequent deformations (see Figs. 4 and 5a). The variation of m is likely to be responsible for the evolution of microstructures in the cyclic tensile deformation, as has been confirmed that the dislocation network is formed and its density reaches saturated after the first tensile deformation.

Conclusions

1. Typical NGSD (10–50 nm) nc-Ni, with an average grain size of 15–25 nm, has a common ductility with δ_{ETF} of $\sim 4\%$ and a high strength with σ_{UTS} of 1200–1300 MPa at RT and strain rates of 3×10^{-3} or 10^{-4} s^{-1} .^{9,11} However, the present BGSD (10–120 nm) nc-Ni sample with an average grain size of 27.2 nm exhibits a considerable ductility with δ_{ETF} over 10% and a similar strength in σ_{UTS} at RT and approaching strain rates.

2. The intracrystalline dislocation network was observed in the post-deformed microstructure, confirming the conventional intracrystalline dislocation sliding mechanism in BGSD nc-Ni. The uniaxial tensile loading–unloading–loading deformation showed that BGSD nc-Ni has the capability to store dislocations in the grain interiors, although it is very limited compared with CG metals.

3. For BGSD nc-Ni, the strain rate sensitivity of flow stress enhances with decreasing strain rate. At the strain rate of $5 \times 10^{-6} \text{ s}^{-1}$, m was estimated to be 0.055. At the corresponding strain rate, the enhanced ductility along with the decreased strength was achievable, indicating activation of other deformation mechanisms, e.g. GB sliding or diffusion at the very slow strain rate.

Acknowledgement

The financial support provided by the Innovation Project of Fuzhou University, the Foundation of Fujian provincial natural science research programme (no. 2008J0145-E0810006) and the National 863 projects of China (no. 2007AA032325) is gratefully acknowledged.

References

1. A. G. Froseth, P. M. Derlet and H. Van Swygenhoven: *Adv. Eng. Mater.*, 2005, **7**, 16–20.
2. M. Chen, E. Ma, K. J. Hemker, H. Sheng, Y. Wang and X. Cheng: *Science*, 2003, **300**, 1275–1277.
3. Z. Shan, E. A. Stach, J. M. K. Wiezorek, J. A. Knapp, D. M. Follstaedt and S. X. Mao: *Science*, 2004, **305**, 654–657.
4. D. Farkas, A. Frosteh and H. Van Swygenhoven: *Ser. Mater.*, 2006, **55**, 695–698.

5. Y. Wang, M. Chen, F. Zhou and E. Ma: *Nature*, 2002, **419**, 912–915.
6. L. Lu, Y. Shen, X. Chen, L. Qian and K. Lu: *Science*, 2004, **304**, 422–425.
7. X. Zhang, H. Wang, R. O. Scattergood, J. Narayan, C. C. Koch, A. V. Sergueeva and A. K. Mukherjee: *Acta Mater.*, 2002, **50**, 4823–4830.
8. R. K. Guduru, L. L. Murty, K. M. Youssef, R. O. Scattergood and C. C. Koch: *Mater. Sci. Eng. A*, 2007, **A463**, 14–21.
9. Y. M. Wang, S. Cheng, Q. M. Wei, E. Ma, T. G. Nieh and A. Hamza: *Scr. Mater.*, 2004, **51**, 1023–1028.
10. X. Shen, J. Lian, Z. Jiang and Q. Jiang: *Mater. Sci. Eng. A*, 2008, **A487**, 410–416.
11. X. L. Wu, Y. T. Zhu and E. Ma: *Appl. Phys. Lett.*, 2006, **88**, (121905), 1–3.
12. Y. B. Wang, B. Q. Li, M. L. Sui and S. X. Mao: *Appl. Phys. Lett.*, 2008, **92**, (011903), 1–3.
13. M. Legros, B. R. Elliott, M. N. Rittner, J. R. Weertman and K. J. Hemker: *Philos. Mag. A*, 2000, **80A**, 1017–1026.
14. Z. Budrovic, H. Van Swygenhoven, P. M. Derlet, S. Van Petegem and B. Schmitt: *Science*, 2004, **304**, 273–276.
15. F. D. Torre, P. Spätig, R. Schäublin and M. Victoria: *Acta Mater.*, 2005, **53**, 2337–2349.
16. P. S. Follansbee and U. F. Kocks: *Acta Metall.*, 1988, **36**, 81–93.
17. J. Lian, C. Gu, Q. Jiang and Z. Jiang: *Appl. Phys. Lett.*, 2006, **99**, (076103), 1–3.
18. A. V. Sergueeva, N. A. Mara and A. K. Mukherjee: *Rev. Adv. Mater. Sci.*, 2004, **7**, 67–74.
19. E. W. Hart: *Acta Metall.*, 1967, **15**, 351–355.
20. Y. M. Wang and E. Ma: *Acta Mater.*, 2004, **52**, 1699–1709.
21. H. Zhang, Z. Jiang, J. Lian and Q. Jiang: *Mater. Sci. Eng. A*, 2008, **A479**, 136–141.
22. Z. Jiang, X. Liu, G. Li, Q. Jiang and J. Lian: *Appl. Phys. Lett.*, 2006, **88**, (143115), 1–3.
23. L. Lu, S. X. Li and K. Lu: *Scr. Mater.*, 2001, **45**, 1163–1169.
24. Y. F. Shen, L. Lu, M. Dao and S. Suresh: *Scr. Mater.*, 2006, **55**, 319–322.